

Transmission Properties of the oscillating delta-function potential

D.F. Martinez and L.E. Reichl
Center for Statistical Mechanics
Department of Physics
The University of Texas at Austin
Austin, TX, 78701, U.S.A

November 2, 2018

Abstract

We derive an exact expression for the transmission amplitude of a particle moving through a harmonically driven delta-function potential by using the method of continued-fractions within the framework of Floquet theory. We prove that the transmission through this potential as a function of the incident energy presents at most two real zeros, that its poles occur at energies $n\hbar\omega + \varepsilon^*$ ($0 < \text{Re}(\varepsilon^*) < \hbar\omega$), and that the poles and zeros in the transmission amplitude come in pairs with the distance between the zeros and the poles (and their residue) decreasing with increasing energy of the incident particle. We also show the existence of non-resonant "bands" in the transmission amplitude as a function of the strength of the potential and the driving frequency.

1 Introduction

Time-dependent potentials in mesoscopic systems have been studied for a number of years in connection with electron-phonon interactions [1], quantum tunneling time [2, 3, 4], ionization [5, 6], electronic transmission [7, 8, 9, 10] and also in the field of quantum chaos [11]. One of the interesting features of localized time-periodic potentials is the presence of resonances or quasi-bound "states", which could be thought of as electrons dynamically trapped by the oscillating potential. This is also a feature common to all multi-channel quantum scattering problems [12, 13].

The solution of any three-term recursion relation, either in functions or in operators, is a continued fraction (C.F.). Such is the case for tight-binding hamiltonians [14, 15], for the time-independent Schrödinger equation (in discretised space) [16], and for harmonic time-dependent potentials, such as an atom in a standing-wave laser field [17, 18] or for tunneling in the presence of phonons [1].

We first prove here, starting from Schrödinger's equation, that the transmission amplitude has the structure of a C.F. of functions of the incident energy and the strength of the delta potential. This is a considerable advantage over the numerical computation of the transmission done before using this kind of potential [7, 8]. Our expression allows us to study with greater detail, both analytically and numerically, several different features of the transmission that had not been noticed or explained before, such as the location of the zero-pole resonances of the transmission and the almost periodic behavior of their position, the existence of non-resonant "bands", the dependence of the pole residues on energy and the existence of the so-called (in the language of nuclear physics) "threshold anomalies" in the transmission. We believe our work gives some insight and clarifies issues in the general problem of scattering through harmonically driven localized potentials. One such potential is the Landau-Büttiker potential, for which numerical and analytical studies of the transmission have been done [9, 10], showing many similarities with the transmission properties of the potential studied in this paper.

In Section 2 we use Floquet's theorem to derive the equations that couple different components of the wave function in a plain wave basis, and then we use these equations to find the S-matrix for this potential. In Section 3 we solve the equations derived in Section 2 and find the exact C.F. expression for the transmission amplitudes. In Section 4 and 5 we study analytically and numerically the zeros and poles of the transmission. In Section 6 we briefly discuss the "threshold anomalies" in the transmission amplitude.

2 Scattering Matrix and Transmission Amplitudes

A formal treatment of the problem of scattering by a time-periodic potential can be found in [9, 19]. Also, a discussion about the sub-space of the Hilbert space suitable for the treatment of time-periodic potentials can be found in [20]. The Hamiltonian we consider is

$$H(x, t) = -\frac{\hbar^2}{2\mu} \frac{d^2}{dx^2} + V\delta(x)\cos(\omega t), \quad (1)$$

where μ is the mass of the particle. Even though energy is not conserved, the Floquet energy, ε , is conserved for this system and takes on a continuous range of values in the interval $0 \leq \varepsilon \leq \hbar\omega$. The Floquet eigenstate with Floquet energy, ε , takes the form

$$\Psi_\varepsilon(x, t) = \sum_{n=-\infty}^{\infty} \psi_n(x) e^{-\frac{i}{\hbar}(\varepsilon + n\hbar\omega)t}. \quad (2)$$

Since the potential is zero everywhere except at $x = 0$, we assume $\psi_n(x)$ to be of the form

$$\psi_n^L(x) = \frac{1}{\sqrt{k_n}}(a_n e^{ik_n x} + d_n e^{-ik_n x}) \quad \text{for } x < 0$$

$$\psi_n^R(x) = \frac{1}{\sqrt{k_n}}(c_n e^{ik_n x} + b_n e^{-ik_n x}) \quad \text{for } x > 0. \quad (3)$$

The factor $\frac{1}{\sqrt{k_n}}$ has been included to ensure unitarity of the S-matrix and the wave-vectors k_n are defined by

$$k_n = \sqrt{\frac{2\mu}{\hbar^2}(\varepsilon + n\hbar\omega)} \quad (4)$$

In this paper n will always have the range $-\infty < n < \infty$. The square root function has its branch cut on the real energy axis (so that a real energy gives a real momentum) and for the energy on the negative real axis we will use the Riemann sheet that has $Im(k_n) \geq 0$, the so called "physical sheet". On this sheet the momentum k_n is on the positive imaginary axis for any $n < 0$. This is required to allow for evanescent modes (exponentially decaying on both sides of the potential) since they can contribute significantly to the wave-function in the neighborhood of the delta function. These evanescent states are also related to resonances or quasi-bound states which are known to exist in multi-channel problems. To avoid any unphysical exponentially growing states when dealing with positive pure imaginary momentum states, we will require that $a_n = 0$ and $b_n = 0$ for $n \leq -1$. To study the resonances in the transmission we will allow the energy to take complex values and will not necessarily stay on the physical sheet. This will be discussed in section 5.

The Floquet eigenstate, $\Psi_\varepsilon(x, t)$, must be continuous at $x = 0$. This leads to the condition that

$$a_n + d_n = c_n + b_n. \quad (5)$$

Because of the delta function in the Hamiltonian, the slope of $\Psi_\varepsilon(x, t)$ is discontinuous and satisfies the condition

$$\left. \frac{d\Psi_\varepsilon}{dx} \right|_{x=0^+} - \left. \frac{d\Psi_\varepsilon}{dx} \right|_{x=0^-} = \frac{2\mu V}{\hbar^2} \cos(\omega t) \Psi_\varepsilon(0, t). \quad (6)$$

This leads to the condition

$$c_n + d_n - b_n - a_n = -2i [h_{n-1}(a_{n-1} + d_{n-1}) + h_n(a_{n+1} + d_{n+1})], \quad (7)$$

where

$$h_n = \frac{\mu V}{2\hbar^2 \sqrt{k_n k_{n+1}}}. \quad (8)$$

We can now combine Eqs. (5) and (7), to obtain the following relations between coefficients

$$c_n + ih_n c_{n+1} + ih_{n-1} c_{n-1} = a_n - ih_n b_{n+1} - ih_{n-1} b_{n-1} \quad (9)$$

and

$$d_n + ih_n d_{n+1} + ih_{n-1} d_{n-1} = b_n - ih_n a_{n+1} - ih_{n-1} a_{n-1}. \quad (10)$$

It is useful to separate the propagating modes from the evanescent modes. Let us define column vectors

$$\bar{c}_p = \begin{pmatrix} c_0 \\ c_1 \\ c_2 \\ \vdots \end{pmatrix} \quad \text{and} \quad \bar{c}_e = \begin{pmatrix} c_{-1} \\ c_{-2} \\ c_{-3} \\ \vdots \end{pmatrix}, \quad (11)$$

where \bar{c}_p contains the amplitudes of the propagating modes outgoing to the right, and \bar{c}_e contains the amplitudes of the evanescent modes that decay to the right. Analogous definitions apply for the column vectors \bar{a}_p , \bar{b}_p , \bar{d}_p , and \bar{d}_e . Note that $\bar{a}_e \equiv \bar{0}$ and $\bar{b}_e \equiv \bar{0}$. We can now rewrite Eqs. (9) and (10) in the following form

$$\begin{aligned} (\bar{1}_{pp} + \bar{X}_{pp}) \cdot \bar{c}_p + \bar{X}_{pe} \cdot \bar{c}_e &= \bar{a}_p - \bar{X}_{pp} \cdot \bar{b}_p, \\ \bar{X}_{ep} \cdot \bar{c}_p + (\bar{1}_{ee} + \bar{X}_{ee}) \cdot \bar{c}_e &= -\bar{X}_{ep} \cdot \bar{b}_p, \\ (\bar{1}_{pp} + \bar{X}_{pp}) \cdot \bar{d}_p + \bar{X}_{pe} \cdot \bar{d}_e &= \bar{b}_p - \bar{X}_{pp} \cdot \bar{a}_p, \\ \bar{X}_{ep} \cdot \bar{d}_p + (\bar{1}_{ee} + \bar{X}_{ee}) \cdot \bar{d}_e &= -\bar{X}_{ep} \cdot \bar{a}_p, \end{aligned} \quad (12)$$

where $\bar{1}_{pp}$ and $\bar{1}_{ee}$ are infinite dimensional unit matrices and matrices \bar{X}_{pp} , \bar{X}_{ee} , \bar{X}_{ep} , and \bar{X}_{pe} have matrix elements

$$\begin{aligned} (\bar{X}_{pp})_{m,m'} &= ih_m (\delta_{m,m'+1} + \delta_{m,m'-1}), & (\bar{X}_{ee})_{\nu,\nu'} &= ih_\nu (\delta_{\nu,\nu'+1} + \delta_{\nu,\nu'-1}), \\ (\bar{X}_{pe})_{m,\nu} &= ih_{-1} \delta_{m,0} \delta_{\nu,-1}, & (\bar{X}_{ep})_{\nu,m} &= ih_{-1} \delta_{m,0} \delta_{\nu,-1}. \end{aligned} \quad (13)$$

Note that we have introduced the convention that the indices $m = 0, 1, 2, \dots, \infty$, and $\nu = -1, -2, -3, \dots, -\infty$, to help separate propagating modes from evanescent modes.

We can now write the scattering matrix for this system. The scattering matrix, \bar{S} , connects the incoming propagating modes to the outgoing propagating modes

$$\begin{pmatrix} \bar{d}_p \\ \bar{c}_p \end{pmatrix} = \bar{S} \cdot \begin{pmatrix} \bar{a}_p \\ \bar{b}_p \end{pmatrix} = \begin{pmatrix} \bar{r} & \bar{t}' \\ \bar{t} & \bar{r}' \end{pmatrix} \cdot \begin{pmatrix} \bar{a}_p \\ \bar{b}_p \end{pmatrix}, \quad (14)$$

where \bar{t} and \bar{t}' are matrices of transmission probability amplitudes and \bar{r} and \bar{r}' are matrices of reflection probability amplitudes. More specifically, the matrix element $t_{m,m'} = (\bar{t})_{m,m'}$ is the probability amplitude for the m' mode entering from the left to transmit to the right, and $r_{m,m'} = (\bar{r})_{m,m'}$ is probability amplitude that the m' mode entering from the left and will reflect to the left. Matrix elements of \bar{r}' and \bar{t}' contain reflection and transmission coefficients for modes entering from the right. After some algebra one can show that

$$\bar{t} = \bar{t}' = (\bar{1}_{pp} + \bar{Y}_{pp})^{-1} \quad \text{and} \quad \bar{r} = \bar{r}' = -(\bar{1}_{pp} + \bar{Y}_{pp})^{-1} \cdot \bar{Y}_{pp}, \quad (15)$$

where

$$\bar{Y}_{pp} = \bar{X}_{pp} - \bar{X}_{pe} \cdot (\bar{1}_{ee} + \bar{Y}_{ee})^{-1} \cdot \bar{X}_{ep}. \quad (16)$$

The effects of the evanescent modes are now explicitly included in the scattering matrix.

For propagating modes entering in the m^{th} channel on the left, the total probability for transmission to the right is

$$T_m = \sum_{m'=0}^{\infty} |t_{m',m}|^2. \quad (17)$$

In the next section we focus on the transmission probability, T_0 . By expanding it in continued fractions, we can determine all the transmission zeros and complex poles of this system.

3 Continued fractions solution

Let us now consider the special case of a single propagating mode, entering in channel $m = 0$ from the left and no propagating modes entering from the right. In this case $a_n = \delta_{n,0}$ and $b_n = 0$. The probability amplitude for the particle to be transmitted into the n^{th} channel (propagating or not) on the right is c_n . For the propagating modes ($n \geq 0$), $c_n = t_{n,0}$. Let us now define the following quantity

$$f_n = \frac{c_n}{c_{n+1}} \quad -\infty < n < \infty \quad (18)$$

In terms of f_n , Eq.(9) gives,

$$1 + \frac{ih_n}{f_n} + ih_{n-1}f_{n-1} = 0 \quad \text{for } n \neq 0 \quad (19)$$

$$1 + \frac{ih_0}{f_0} + ih_{-1}f_{-1} = \frac{1}{c_0} \quad \text{when } n=0 \quad (20)$$

For $n \geq 0$ we can write the solution of (19) in the form

$$f_n = \frac{1}{-ih_n} \left(1 + \frac{ih_{n+1}}{f_{n+1}} \right) \quad (21)$$

or,

$$f_n = \frac{1}{-ih_n} \left(1 + \frac{h_{n+1}^2}{1 + \frac{h_{n+2}^2}{1 + \frac{h_{n+3}^2}{\ddots}}} \right) \quad (22)$$

For $n \leq -1$ we write the solution in the form

$$f_n = \frac{-ih_n}{1 + ih_{n-1}f_{n-1}} \quad (23)$$

or,

$$f_n = \frac{-ih_n}{1 + \frac{h_{n-1}^2}{1 + \frac{h_{n-2}^2}{1 + \frac{h_{n-3}^2}{\ddots}}}} \quad (24)$$

From the above expressions for the f_n 's (when $n = 0$ and $n = -1$) we can obtain c_0 from Eq.(20),

$$c_0 = t_{0,0} = \frac{1}{1 + \frac{i\hbar_0}{f_0} + ih_{-1}f_{-1}} = \frac{1}{1 + \frac{h_0^2}{1 + \frac{h_1^2}{1 + \frac{h_2^2}{1 + \frac{h_3^2}{1 + \frac{h_{-2}^2}{1 + \frac{h_{-3}^2}{1 + \frac{h_{-4}^2}{\ddots}}}}}}}} \quad (25)$$

With the solution for the f_n 's and c_0 known, any coefficient c_n can be found (using Eq.18) in the following way,

$$c_n = \frac{c_0}{f_{n-1}f_{n-2}\dots f_0} \quad \text{for } n \geq 1$$

and

$$c_n = f_n f_{n+1} \dots f_{-1} c_0 \quad \text{for } n \leq -1 \quad (26)$$

From here, the transmission probability, T_0 , can be written as

$$T_0 = \sum_{n=0}^{\infty} |c_n|^2 = |t_{0,0}|^2 \left(1 + \sum_{n=1}^{\infty} \frac{1}{\prod_{n'=1}^n |f_{n'-1}|^2} \right) = |t_{0,0}|^2 S(\varepsilon, V). \quad (27)$$

As it can be seen in Fig. 1, none of the f_n 's (for $n \geq 0$) appear to have zeros in the half-plane $\text{Re}[\varepsilon] > 0$. This implies that the function $S(\varepsilon, V)$ has neither zeros nor poles in that region; consequently, the zeros and poles in the transmission probability are the zeros and poles of $|t_{0,0}|^2$. From now on we concentrate on $t_{0,0}$ only.

4 Transmission Zeros

The coefficient c_0 can be taken to be a continuous function of the incoming energy $E = \varepsilon + n\hbar\omega$, instead of a function of the Floquet energy ε . This is so because, when the incident energy is in channel m ($E = m\hbar\omega + \varepsilon$), we need to solve Eq.(9) with the condition $a_n = \delta_{n,m}$. The solution is given in terms of the coefficient c_m which now plays the former role of c_0 . The C.F. for c_m is given by Eq.(25) with m added to all subscripts. As it can be seen easily, $c_m(\varepsilon) = c_0(m\hbar\omega + \varepsilon) = c_0(E)$, which means that the general solution of the problem, for any incoming energy can be obtained from the C.F. expression for c_0 derived in Eq.(25) evaluating it at any energy E . Notice also that $c_0(E) = c_0(m\hbar\omega + \varepsilon) = t_{m,m}(\varepsilon)$. Because of this, and to be rigorous with the notation, we define $t_0(E) = t_0(m\hbar\omega + \varepsilon) \equiv t_{m,m}(\varepsilon) = c_0(E)$. From this we can say that $t_0(E)$ contains the same information as the whole diagonal of the transmission matrix \bar{t} in Eq.(14).

To study the properties of $c_0(E)$ it is convenient to define the following quantities (see Eq. 8)

$$g_n(\epsilon) \equiv h_n^2(\epsilon) = \frac{a}{\sqrt{\epsilon+n}\sqrt{\epsilon+n+1}}$$

with dimensionless parameters

$$a \equiv \frac{mV^2}{8\hbar^3\omega}, \quad \epsilon \equiv \frac{\varepsilon}{\hbar\omega}$$

and

$$e \equiv \frac{E}{\hbar\omega} = \epsilon + n \quad \text{for} \quad n\hbar\omega \leq E \leq (n+1)\hbar\omega \quad (28)$$

Also, we define the function

$$F_0(e) = F_0(n+\epsilon) \equiv F_n(\epsilon) \equiv 1 + i \frac{h_0(n+\epsilon)}{f_0(n+\epsilon)} = 1 + \frac{g_n(\epsilon)}{1 + \frac{g_{n+1}(\epsilon)}{1 + \frac{g_{n+2}(\epsilon)}{\ddots}}} \quad (29)$$

Notice that $g_n(\epsilon)$ also depends on a .

Using the definitions given above we can write the coefficient $c_0(e)$ for the range $n \leq e \leq (n+1)$, in the following way

$$c_0(e) = c_0(n+\epsilon) = \frac{1}{F_n(\epsilon) + \frac{g_{n-1}(\epsilon)}{1 + \frac{g_0(\epsilon)}{1 + \frac{g_{-1}(\epsilon)}{1 + \frac{g_{-2}(\epsilon)}{\ddots}}}}} \quad (30)$$

In the above expression all quantities are real (for ϵ real) except for $g_{-1}(\epsilon)$ which is pure imaginary. This has an important consequence for the number of real zeros in $c_0(e)$ as we shall see next.

Let us rewrite the equation above in a slightly different way:

$$c_0(n+\epsilon) = \frac{1}{F_n(\epsilon) + \frac{g_{n-1}(\epsilon)}{1 + \frac{g_{n-2}(\epsilon)}{1 + \frac{g_0(\epsilon)}{1 + iG(\epsilon)}}}} \quad (31)$$

where the continued fraction $G(\epsilon)$ is defined as

$$G(\epsilon) \equiv \frac{-a}{\sqrt{1-\epsilon}\sqrt{\epsilon}\left(1 + \frac{g_{-2}(\epsilon)}{1 + \frac{g_{-3}(\epsilon)}{\ddots}}\right)} \quad (32)$$

Notice $G(\epsilon)$ is a real function for ϵ real and $0 \leq \epsilon \leq 1$.

If Eq. (31) is put in the form of a standard fraction, we get

$$c_0(\epsilon) = \frac{1}{F_0 + iG} \quad \text{for } n=0$$

and

$$c_0(n + \epsilon) = \frac{iP_n(g_{n-2}, g_{n-3}, \dots, g_0)G + R_n(g_{n-2}, g_{n-3}, \dots, g_0)}{iQ_n(F_n, g_{n-1}, \dots, g_0)G + S_n(F_n, g_{n-1}, \dots, g_0)} \quad \text{for } n>0 \quad (33)$$

In the last expression, P_n, Q_n, R_n, S_n are polynomials on the variables g_n and F_n indicated in parentheses, such that the coefficient of every term is equal to one and all variables appear elevated to the first power only (i.e. $1 + g_1 + g_1g_2 + \dots$). Notice that G is the only function that can take values between $-\infty$ to ∞ . The other functions (F_n and g_n) are strictly positive and finite for $\epsilon > 0$. This implies that P_n, Q_n, R_n, S_n are strictly positive and finite, which means that, for $n > 0$, the numerator of c_0 can never be zero and the denominator does not go to infinity unless $G \rightarrow \infty$, in which case the numerator would also blow up keeping the fraction strictly positive. From this we can conclude that *there are no real transmission zeros for incident energies $E > \hbar\omega$.*

For $n=0$ we see that a real zero can only happen when $F_0(\epsilon, a) \rightarrow \infty$ or $G(\epsilon, a) \rightarrow \infty$. The first case only occurs when $\epsilon = 0$ (G blows up at this point too). For the second case, the real zeros of $t_0(\epsilon, a)$ are given by the zeros of $G^{-1}(\epsilon, a)$. As it can be seen from Fig. 2 the function $G^{-1}(\epsilon, a)$ seems to have some periodicity. This can also be seen in Fig. 3 where the curves $\delta(a)$ that satisfy $t_0(\delta, a) = G^{-1}(\delta, a) = 0$ are shown. This dependence of the transmission real zeros with the parameter a can be seen directly in Fig. 4 in the sequence of transmission graphs for different values of the strength of the delta.

It is interesting to notice in Fig. 3 and Fig. 4 that there are intervals of a , around integer values, for which the real zero in the transmission disappears. A table (for $0 \leq a \leq 9$) with the exact values (to seven digits) of the intervals for which there is a real zero in the transmission (apart from the trivial one at $E = 0$) is shown in Table 1. This behavior of the real zero seems to be matched by the behavior of the poles of the transmission as we will see next.

5 Transmission Poles

In this section we prove by induction that the poles of $c_0(e)$ occur at energies $e = (n + \epsilon^*)$ with $0 < Re(\epsilon^*) < 1$ and show that their residue decreases with

increasing n (energy). We start with equation (30) and write it in the form

$$c_0(n + \epsilon) = \frac{1}{F_n(\epsilon) + G_n(\epsilon)} \quad (34)$$

where F_n and G_n satisfy

$$\begin{aligned} F_n(\epsilon) &= 1 + \frac{g_n(\epsilon)}{F_{n+1}(\epsilon)} \\ G_n(\epsilon) &= \frac{g_{n-1}(\epsilon)}{1 + G_{n-1}(\epsilon)} \end{aligned} \quad (35)$$

Let's assume that $c_0(e)$ has a pole at $e = n + \epsilon^*$. This implies that $c_0(e)$ has also a pole at $e = n + 1 + \epsilon^*$ because we can write from Eqs. (34) and (35)

$$\begin{aligned} c_0(n + 1 + \epsilon) &= \frac{1}{F_{n+1}(\epsilon) + G_{n+1}(\epsilon)} \\ &= \frac{1}{\frac{g_n(\epsilon)}{F_n(\epsilon) - 1} + \frac{g_n(\epsilon)}{1 + G_n(\epsilon)}} \\ &= \frac{(1 + G_n(\epsilon))(F_n(\epsilon) - 1)}{g_n(\epsilon)(F_n(\epsilon) + G_n(\epsilon))} \\ &= \frac{(1 + G_n(\epsilon))}{F_{n+1}(\epsilon)(F_n(\epsilon) + G_n(\epsilon))} \end{aligned} \quad (36)$$

It is important to notice that, since $f_0(e)$ (as shown in Fig.1) has neither poles nor zeros in the half plane $Re(e) > 0$, the function $F_n(\epsilon) = F_0(n + \epsilon) = 1 + i \frac{h_0(\epsilon)}{f_0(\epsilon)}$ does not have poles and $F_n(\epsilon) \neq 1$. This implies that (from the last line of Eq. (36)) if $c_0(e)$ has a pole at $n + \epsilon^*$ (which means that $F_n(\epsilon^*) + G_n(\epsilon^*) = 0$), then it must have a pole at $n + 1 + \epsilon^*$ (The numerator in Eq. (36) does not vanish at $\epsilon = \epsilon^*$ because $G_n(\epsilon^*) = -F_n(\epsilon^*) \neq -1$).

Notice also that when $n \rightarrow \infty$, $F_n \rightarrow 1$, because $f_0(n + \epsilon) \rightarrow \infty$, and $h_0(n + \epsilon) \rightarrow 0$ in this limit. This means that the location of the transmission zero approaches the location of the pole as the incoming energy grows; the zero happens when $\epsilon = \delta$, with $G_n(\delta) = -1$; the pole occurs when $\epsilon = \epsilon^*$, with $G_n(\epsilon^*) = -F_n(\epsilon^*)$. Obviously $\delta \rightarrow \epsilon^*$ because $F_n(\epsilon^*) \rightarrow 1$ as $n \rightarrow \infty$. From that we conclude that the residue of the poles in the transmission amplitude tend to zero as $n \rightarrow \infty$. This explains why, even though the transmission amplitude has an infinite number of poles separated by a distance of $\hbar\omega$ in the incoming energy, all at the same distance from the real axis, only the effect of the first poles can be seen in the graphs of transmission probability versus incoming energy. Another way to say this is that the zeros (in the complex plane) at higher energies are very close to the poles, therefore canceling out the possible effect of the poles in the transmission.

In Fig. 5 we show a graph of the imaginary part of $t_0(e)$ where the poles in channels 0, 1, 2, can be seen (we refer to channel n as the strip in the complex energy plane that satisfies $n < \text{Re}(e) < n + 1$). It is evident in that graph that the poles have support on different sheets; we will call these sheets S_n , where n refers to the channel number. This sheeted structure comes from the fact that, because the functions $k_n(e)$ have a branch point at $e = -n$ and two Riemann sheets, any function of $k_n(e)$ ($t_0(e)$ in particular) will have a multiple-sheeted structure. What is called the "physical" sheet (P) in the context of multiple channel scattering is the sheet obtained when selecting all the Riemann sheets with $\text{Im}(k_n) > 0$. Each sheet of the full multi-sheeted surface can be labeled by the sequence of signs of $\text{Im}(k_\infty), \dots, \text{Im}(k_1), \text{Im}(k_0), \text{Im}(k_{-1}), \dots, \text{Im}(k_{-\infty})$, e.g., (+..-+..+) (bold has been used to indicate the sign of $\text{Im}(k_0)$); fortunately we do not need to consider all these sheets, since only a small fraction of them are of physical interest; the principal one being P or (+..+..+). Crossing the real axis from P at an energy $m < e < m + 1$ crosses all the branch cuts whose branch point is at an energy smaller than $e = m$ (see figure 6). The sheet that is the smooth continuation of P into the lower complex plane (smooth even at the cut) is the one obtained by taking $\text{Im}(k_{-n}) < 0$ for all $n \leq m$ and $\text{Im}(k_{-n}) > 0$ for all $n > m$. We call these sheets S_m and they are precisely the ones where the poles in the transmission are found, as shown schematically in Fig. 7.

Resonances, as opposed to bound state poles, do not occur in the "physical" sheet; however, from the unitarity of the S-matrix extended to the complex plane, they can have important effects on the behavior of the S-matrix along the real axis (see [12] for an excellent discussion on multiple channel scattering).

In single channel scattering, the unitarity of the S-matrix on the real axis has consequences in the analytic structure of the S-matrix in both sheets, the most important one being the zero-pole structure of the resonances: every pole has a companion zero at a position complex conjugate to the position of the pole but on a different sheet. For multiple channel scattering the position of the pole and zero are not so simply related and often the pole and zero appear in the same sheet.

The position of the pole (e^*) in the first channel, can be found by looking at the zeros of the function $F_0(e, a) + G_0(e, a)$ with the appropriate selection of Riemann sheets, as described before, so as to be on the sheet S_0 . A graph of the position of the pole as the strength of the potential is varied is shown in Fig. 8, where it can be seen that the pole approaches the real axis at $e^* = 1$ when $a \rightarrow 0$, annihilating the real zero which also goes to the same position with $a \rightarrow 0$. As the parameter a is increased the zero moves to the left on the real axis (see Fig. 3) and the pole moves away from the real axis describing an arch. At $a = a_0^h = 0.7821147$ (all values of a are accurate to the seventh digit) the zero disappears at $\delta = 0$ and so does the pole. For values of a slightly greater, the transmission has a very high peak but it is not a pole, as can be seen in Fig. 9 (compare with the pole at $a = 0.78$ in Fig. 10). In the interval $a_0^h < a < a_1^l$ the transmission does not have any zero-pole resonances. In this interval the peak or false "pole" follows a trajectory that seems the continuation

of the trajectory the pole had followed until it vanished. When $a = a_1^l$ the zero reappears on this channel, entering at $\delta = 1$. At this value however, we do not see any pole in this channel. There is in fact a pole on S_0 but it is located in the next channel ($1 < \text{Re}(e^*) < 2$). For $a \approx 1.3$ the pole has finally made it into the $n = 0$ channel. As a is further increased the pole continues to describe an arch until it disappears along with the zero. A similar behavior to the one described above occurs for increasing values of the parameter a , with the pole describing ever increasing arches, each one farther away from the real axis than the previous one. An identical behavior of the poles on other sheets is expected from the discussion following Eq.(36).

This quasi-periodic behavior of the transmission resonances as a function of the strength of the oscillating potential and the driving frequency has not been found before. Around integer values of a the oscillating potential seems to be incapable of dynamically trapping particles not even for a short period of time.

6 Threshold anomalies

One of the most evident features in the transmission versus energy curves for all values of a is what seems to be a discontinuity in the slope at $e = n\hbar\omega$ (channel openings). A close look into this regions reveals that there is a rapid divergence of the slope at the thresholds, that is, $\frac{dt_0}{de} \rightarrow \pm\infty$ as $e \rightarrow n\hbar\omega$. This is actually a common occurrence in all multi-channel scattering problems, and it can be traced back to the fact that when the energy is in the n^{th} channel near threshold, the first open-channel momentum is $k_{-n} = \sqrt{e - n\hbar\omega}$. It can be proven that the S-matrix has elements that are linear functions of this momentum near threshold. This clearly implies that the derivative of these elements with respect to the energy must diverge at threshold (for more details see [21]). These threshold anomalies can easily be proven to exist in our particular time dependent potential by looking at our C.F. solution for $t_0(e)$ in Eq. 25. From it, it is clear that the derivative of this expression gives an infinite number of terms, each one proportional to the derivative of some function $g_n(e)$. These functions and their derivatives diverge at their thresholds (see the expression for g_n in Eq. 28), therefore the derivative of $t_0(e)$ must also diverge at each threshold. According to this, the shape of the threshold anomaly can be of four different kinds, two cusps like and two rounded steps, as shown in Fig. 11. These four different kinds of anomalies are shown in Fig. 12 as they occur in the $|t_0(e)|$ graphs for two different values of a .

7 Conclusions

The exact solution for the problem of transmission of a particle through a monochromatic oscillating potential has been found with the use of C.F's. This approach represents a significant improvement over the standard method which can only be carried out numerically since it involves the inversion of an infinite

tri-diagonal matrix, which can be a computationally demanding problem when studying the zero-pole structure of the transmission on the complex plane. The efficiency of the C.F. method allowed us to perform, in a short time, calculations that required including processes of phonon emission and absorption of 65th order (for $a = 9$) which would have required in the standard method the computation of a 131×131 S-matrix for every point in the complex plane where the transmission is to be evaluated. Most importantly, it allowed us to prove rigorously some general properties of the transmission for this system, such as the existence of transmission zeros only in the first channel, the location of the poles at regular intervals of $\hbar\omega$ in the incident energy, the decrease in the residue of the poles with increasing energy, and also allowed us to understand the existence of threshold anomalies at the channel openings.

The study of the behavior of the poles and real zeros as a function of the parameter $a = \frac{mV^2}{8\hbar^3\omega}$ showed an interesting quasi-periodic dependence on a and the presence of "bands" of non-resonant values of a for which the transmission does not have zero-pole resonances. It can also be mentioned that the life-time of the quasi-bound states decreases with increasing a , which can be accomplished by either increasing the strength V of the potential or by decreasing the frequency of the oscillations.

The scattering of particles through a time-periodic potential is another example of multi-channel scattering, for which a great deal of theory and research has been done in the past and still continues to be an important topic of research. In this paper we have put Floquet scattering in the greater context of multi-channel scattering to which it belongs and by doing so we believe some aspects of the transmission through oscillating (localized) potentials have been clarified.

Even though these results were derived for an oscillating delta potential, a similar behavior can be expected to be found for other oscillating finite-range potentials such as the Landauer-Büttiker potential, since this potential reduces to the oscillating delta in an appropriate limit, and also because several common features can already be observed when comparing the transmission curves for this two potentials (see [9]). The exact solution for the oscillating delta plus a static (attractive or repulsive) delta potential can be found using the same C.F. method. The transmission through this potential has been studied numerically before [7], showing features similar to the ones discussed here with the main difference been that the location of the resonances is displaced by an amount of energy roughly equal to the energy of the bound state associated with the static part of the potential.

8 Acknowledgements

The authors wish to thank the Welch Foundation, Grant No.F-1051, NSF Grant INT-9602971 and DOE contract No.DE-FG03-94ER14405 for partial support of this work.

References

- [1] B.Y. Gelfand, S. Schmitt-Rink, A.F.J. Levi, Phys.Rev.Lett., 62, 1683(1989).
- [2] M. Büttiker, R. Landauer, Phys.Rev.Lett., 49, 1739(1982).
- [3] J.A. Stovneng, E.H. Hauge, J.Stat.Phys., 57, 841(1989).
- [4] T. Tanizawa, J.Phys.Soc.Japan, 65, 3157(1996).
- [5] F. Bench, H.J. Korsch, N. Moiseyev, J.Phys.B, 24, 1321(1991).
- [6] O. Costin, J.L. Lebowitz, A. Rokhlenko, J.Phys.A, 33, 6311(2000).
- [7] P.F. Bagwell, R.K. Lake, Phys.Rev.B, 46, 15329(1992).
- [8] E. Cota, J.V. Jose, F.Rojas, Nanostructured Materials, 3, 349(1993).
- [9] W. Li, L.E. Reichl, Phys.Rev.B, 60, 15732(1999).
- [10] M. Wagner, Phys.Rev.A, 51, 798(1995).
- [11] L.E. Reichl in *The Transition to Chaos in Conservative Classical Systems: Quantum Manifestations*, (Springer-Verlag, New York, 1992).
- [12] K.W. McVoy in *Fundamentals in Nuclear Theory*, edited by A. De-Shalit and C. Villi, (International Atomic Agency, Vienna, 1967).
- [13] P.F. Bagwell, A. Kumar, R.K. Lake in *Quantum Effect Physics, Electronics and applications*, edited by K. Ismail et al., (Adam-Hilger, Bristol, 1992).
- [14] B. Kónya, G. Lévai, Z. Papp, J.Math.Phys., 38, 4832(1997).
- [15] S.G. Davison, R.A. English, Z.L. Miskovič, F.O. Goodman, A.T. Amos, and B.L. Burrows, J.Phys.-Cond.Mat. 9, 6371(1997).
- [16] J.P. Vigneron, Ph. Lambin, J. Phys.A: Math. Gen. 13, 1135(1980).
- [17] S.H. Autler, C.H. Townes, Phys.Rev., 100, 703(1955).
- [18] K. Berg-Sorenson, Y. Castin, E. Bonderup, K. Molmer, J.Phys.B, 25, 4195(1992).
- [19] D.S. Saraga, M. Sassoli-de-Bianchi, Helv.Phys.Acta, 70, 751(1997).

- [20] H. Sambe, Phys.Rev.A, 7, 2203(1972).
- [21] R.G. Newton in *Scattering theory of waves and particles*, (McGraw-Hill, New York, 1966).

	l	h
a_0	0	0.7821147
a_1	1.1652568	1.7710590
a_2	2.1873508	2.7667368
a_3	3.1979937	3.7642963
a_4	4.2045658	4.7626808
a_5	5.2091415	5.7615115
a_6	6.2125623	6.7606150
a_7	7.2152455	7.7598995
a_8	8.2174231	8.7593115

Table 1: Intervals of $a = \frac{mV^2}{8\hbar^3\omega}$ for which a zero-pole resonance can be found in the system. The notation a_n^l/a_n^h (used in the text and in some graphs) refers to the lower/higher value of the interval a_n .

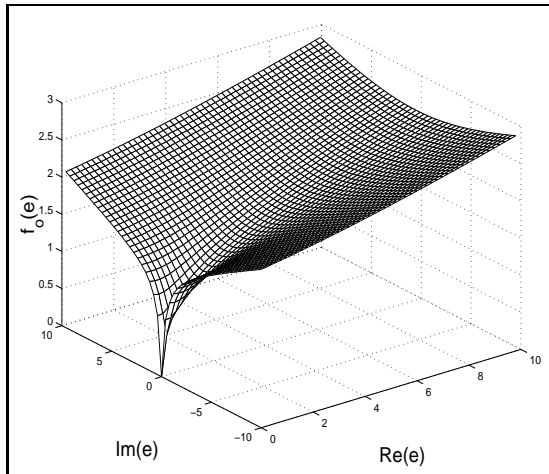


Figure 1: Graph of $|f_0(E)|^2$ in the complex plane (E in units of $\hbar\omega$). $a = 10$. Notice that $f_n(\varepsilon) = f_0(n + \varepsilon) = f_0(E)$, therefore this graph shows the behavior of $f_n(\varepsilon)$ for $0 \leq n \leq 9$. The function behaves similarly, but with a different scale, for other values of a .

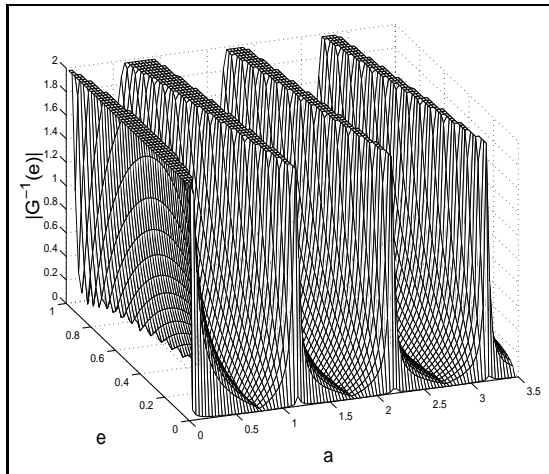


Figure 2: Graph of the function $|G^{-1}(\epsilon, a)|$. The zeros of this function give the real zeros of the transmission.

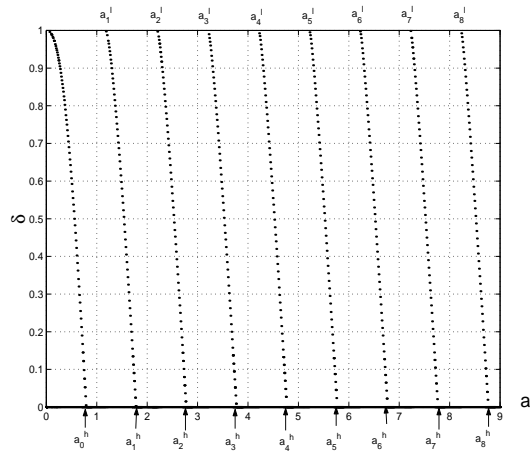


Figure 3: Location of the real zero of t_0 as a function of a .
 $t_0(\delta, a) = G^{-1}(\delta, a) = 0$.

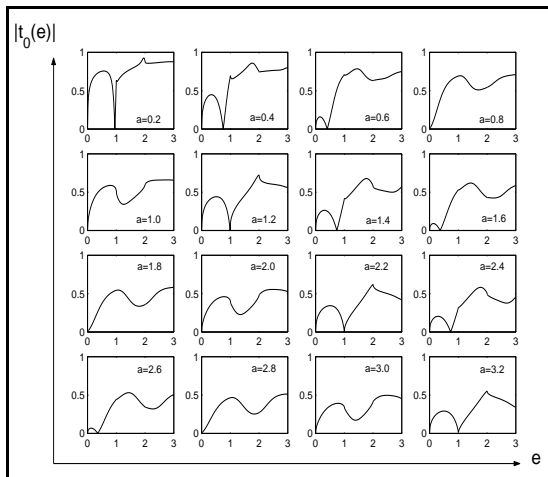


Figure 4: Sequence of $|t_0(e)|$ graphs for increasing values of a showing the evolution of the transmission real zeros.

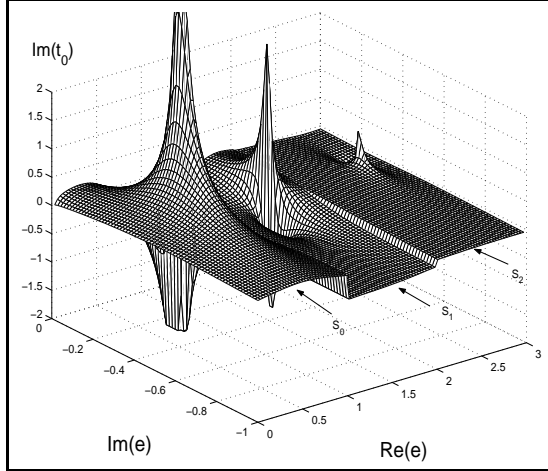


Figure 5: Graph of the imaginary part of $t_0(e)$ for $a=0.5$, showing several poles. Each pole is located on a different sheet.

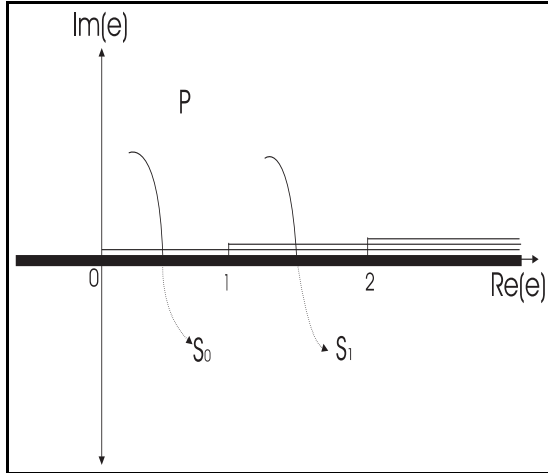


Figure 6: top view of the physical sheet P and the threshold branch points and cuts in the complex energy plane. Indicated with a thin line are the branch cuts corresponding to the branch points $n = 0, 1, 2$; the thick line represents all the branch cuts with branch point at negative energy ($n < 0$ branch points). Paths that start on the upper half of P and go under the branch cut lead to the different sheets S_n (which in this figure are assumed to be underneath P).

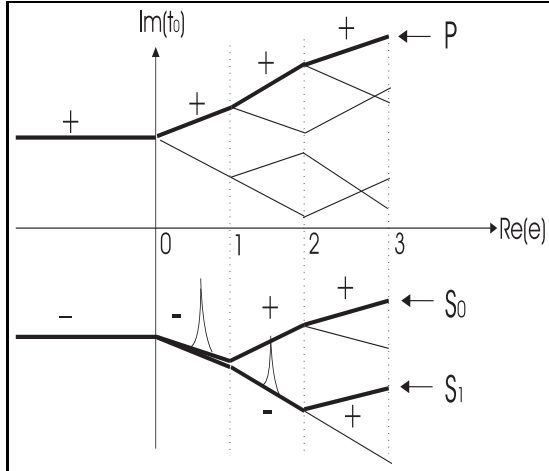


Figure 7: Sketch of $Im(t_0(e))$ versus $Re(e)$ (we assume $Im(e) = constant < 0$) which gives a schematic representation of the different sheets where the poles of the transmission are located. The peak structures in the lower part of the figure represent poles.

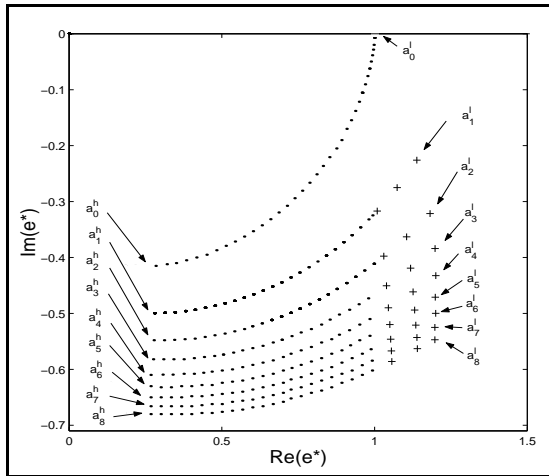


Figure 8: Trajectory of one of the transmission poles as a is changed from 0 to 9. Here a_n^l/a_n^h refers to the lower/higher value of the interval a_n given in Table 1.

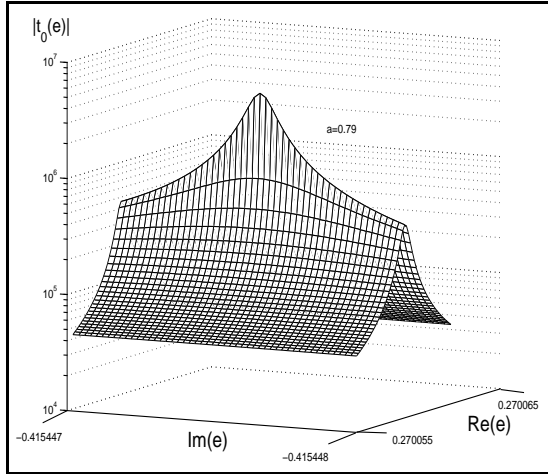


Figure 9: false "pole" of $t_0(e)$ for $a = 0.79$, right after the zero has disappeared at $\delta = 0$ for $a = a_0^h$.

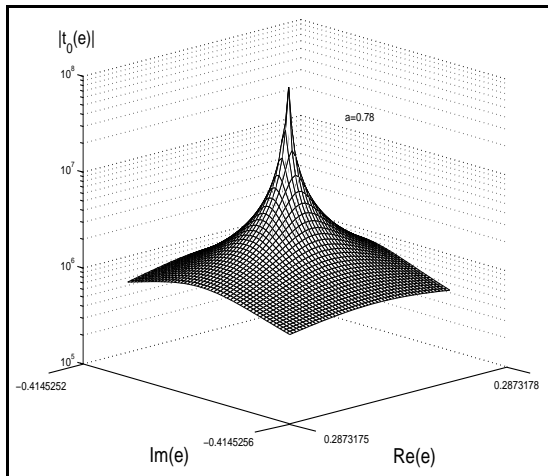


Figure 10: True pole of the transmission for $a = 0.78$, slightly lower than the value of a ($a = a_0^h$) for which the zero disappears.

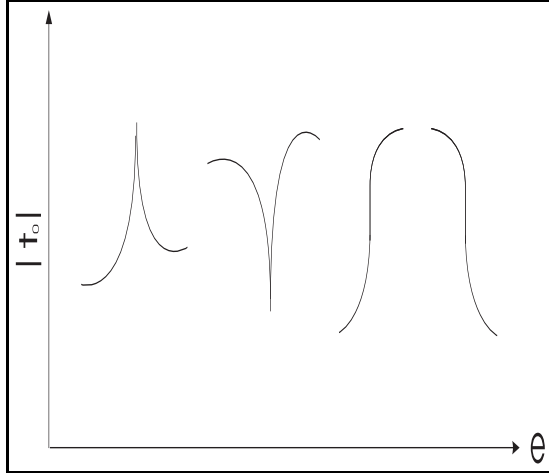


Figure 11: Various forms of transmission amplitude behavior at a channel opening.

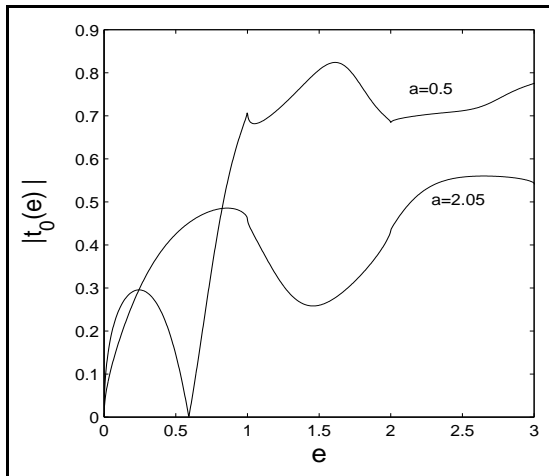


Figure 12: Graph of $|t_0(e)|$ vs. incoming energy. Threshold anomalies of "cusp" type at the channel openings for $a=0.5$. Threshold anomalies of "rounded step" type for $a=2.05$.